ECDP: Energy Consumption Disaggregation Pipeline for Energy Optimization in Lightweight Robots

Juan Heredia, Robin Jeanne Kirschner, Christian Schlette,
Saeed Abdolshah, Sami Haddadin, and Mikkel Baun Kjægaard

***Abstract*—Limited resources and resulting energy crises occurring all over the world highlight the importance of energy efficiency in technological developments such as robotic manipulators. Efficient energy consumption of manipulators is necessary to make them affordable and spread their application in the future industry. Previously, the power consumption of the robot motion was the main factor considered in the evaluation of energy efficiency. Lately, the paradigm in industrial robotics shifted towards lightweight robot manipulators which require a new investigation on the disaggregation of robot energy consumption. In this paper, we propose a novel pipeline to identify and disaggregate the energy use of mechatronic devices and apply it to lightweight industrial robots. The proposed method allows the identification of the electronic components consumption, mechanical losses, electrical losses, and required mechanical energy for robot motion. We evaluate the pipeline and understand the distribution of energy consumption using four different manipulators, namely, Universal Robot's UR5e, UR10e, Franka Emika's FR3, and Kinova Gen3. The experimental results show that most of the energy (60–90 %) is consumed by the electronic components of the robot control box. Using this knowledge, the approaches to further optimize their energy consumption need to shift towards efficient robot electronic design instead of efficient robot mass distribution or motion control. Finally, our disaggregation pipeline allows an understanding of the power consumption of any mechatronic device and thus enables deliberate optimization of energy consumption.**

***Index Terms*—Energy and environment-aware automation. industrial robots, engineering for robotic systems.**

I. Introduction

LIGHTWEIGHT Industrial Robots (LIRs) are an essential part of industrial automation and supply chain optimization for the industry of the future [1], [2]. They can operate alongside workers and improve production quality, worker safety, and labor shortage by taking on highly accurate, repeatable, or hazardous tasks [2]. As a result, the number of new collaborative robots increases yearly, e.g., by 50 % in 2021 [1]. The Energy Consumption (EC) of LIRs is indeed smaller than their heavier, high-payload counterparts. However, we posit that the smaller window for energy savings in lightweight industrial robots should not undermine its significance. Even marginal energy savings per unit, when extrapolated across thousands of robots, can result in considerable energy conservation at larger scales. Significant efforts have been applied to traditional industrial manipulators to optimize EC by minimizing the mechanical energy required for motion, such as in trajectory planning [3], [4]. However, when it comes to optimizing the EC of LIRs, the mechanical motion energy might not be a sufficient parameter. This is because LIRs have a lighter, more flexible structure, which requires less mechanical energy for movement in comparison to the required electrical energy. LIRs are equipped with numerous sensors, such as torque, current sensors, in conjunction with advanced control algorithms. These enhancements aid in collision detection and safe human-robot interaction, thereby ensuring secure human-robot co-working environments. It is anticipated that the EC associated with the electronics of LIRs will be greater compared to their counterparts. Identifying the optimization parameters for the LIR's energy efficiency, thus, requires selective disaggregation and modeling of the EC.

In this letter, we introduce the *energy consumption disaggregation pipeline (ECDP)* to identify and disaggregate the EC of robot manipulators. For this, we propose a model that splits the

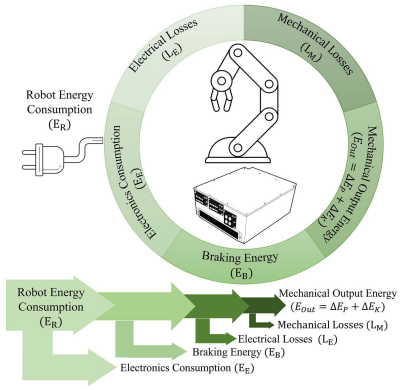

Fig. 1. Energy Consumption Disaggregation Pipeline (ECDP) of Lightweight Industrial Robots: Method to divide the energy consumption of a robot in five principal consumer groups: Output Mechanical Energy E_M, Mechanical Losses L_M, Electrical Losses L_E, Braking Energy E_B, and Electronics Components Consumption E_E.

Manuscript received 15 February 2023; accepted 16 July 2023. Date of publication 3 August 2023; date of current version 16 August 2023. This letter was recommended for publication by Associate Editor J. Kim and Editor H. Moon upon evaluation of the reviewers' comments. This work is part of the project "Industry 4.0 lab facilities for Experimenting with Spatial and Electricity Consumption Data", which was supported in part by the Lighthouse Initiative KI.FABRIK Bayern by StMWi Bayern, Forschungs- und Entwicklungsprojekt, under Grant DIK0249, and in part by the Bavarian State Ministry for Economic Affairs, Regional Development and Energy (StMWi) as part of the project SafeR-oBAY under Grant DIK0203/01. Please note that S. Haddadin has a potential conflict of interest as a shareholder of Franka Emika GmbH. *(Corresponding author: Juan Heredia.)*

Juan Heredia, Christian Schlette, and Mikkel Baun Kjægaard are with Maersk Mc-Kinney Moller Institute, University of Southern Denmark, 5230 Odense, Denmark (e-mail: jehm@mmmi.sdu.dk; chsch@mmmi.sdu.dk; mbkj@mmmi.sdu.dk).

Robin Jeanne Kirschner, Saeed Abdolshah, and Sami Haddadin are with the Munich Institute of Robotics and Machine Intelligence, Technical University of Munich, 80992 Munich, Germany (e-mail: robin-jeanne.kirschner@tum.de; saeed.abdolshah@tum.de; haddadin@tum.de).

Digital Object Identifier 10.1109/LRA.2023.3301311

EC into five groups of electronic consumers and sources of EC, as depicted by Fig. 1: Electrical Losses, Mechanical Losses, Output Mechanical Energy, Braking Energy, and Electronic Components' Consumption. Then, we apply the pipeline to four LIRs Universal Robot UR5e, UR10e, Franka Emika FR3, and Kinova Gen3. Following, we analyze the distribution of EC for LIRs and discuss the resulting parameters for energy optimization in LIR design and control. Finally, we propose novel optimization strategies for LIR EC.

This letter is structured as follows. Section II summarizes techniques to analyze the EC of robot manipulators. In Section III, we define a model for EC. In Section IV, we describe the ECDP, and in Section V, we present the results of the method applied to the following robots, UR5e, UR10e, FR3, and Gen3. In Section VI, we analyze the results of the experiments and propose new perspectives on how to optimize EC. Finally, Section VII concludes this work.

II. State of the Art

Previously, EC of manipulators was analyzed using two methods: 1) mathematical models, e.g., [4], [5], [6], [7], [8], [9], [10], [11], [12] and 2) inductive models based on experiments [3], [13], [14], [15], [16].

EC models for industrial robots (IRs) were developed based on the mechanical energy required to move the robot in [4], [5], [7], [9]. Furthermore, the EC of the electrical components of the drive system was included in the models by [6], [8], [10], [11], [12], [17]. However, the EC of the other components such as the controller (onboard computer), joint microcontrollers, sensors, and ventilators are ignored, and the inaccuracy of existing energy models results in a strong deviation between simulations and real power consumption [3]. Besides, the models have been trained and developed for traditional IRs. The accuracy of the models might decrease when they are tested in LIRs because the EC of the components ignored in the traditional models is important. In [18], an EC model for LIRs which includes the EC of electronic elements was presented.

In the second approach, authors have proposed experimental procedures to analyze the effect of operational factors, such as stand-by positions, payload, velocity limits, acceleration limits, and others on the EC. For example, the payload influence on the energy increment is quantified [4], [5], [7], [13], [14], [15] and the relationship between joint configuration in defined stand-by positions and robot EC was investigated by [14]. Research groups also analyzed the relationship between acceleration and velocity limits to the EC [3], [6], [13], [14], [17]. The temperature of the motors has been examined in [3], [14], showing that the EC is inversely proportional to the temperature. Lastly, the effect of the release of joint brakes, which are mechanisms used to maintain the robot's position on EC was shown in [3], [6], [8], [14].

These two approaches qualitatively analyze the EC, but they do not quantify and disaggregate the energy use of the manipulator components. Energy disaggregation is a method traditionally used in building science for analyzing and optimization of EC on buildings [19]. To the best of the authors' knowledge, this method to examine the EC has not yet been applied to quantify and methodically disaggregate the EC of mechatronic devices, especially LIRs. However, such analysis is required to improve the energy efficiency of LIRs.

III. Energy Model of a Manipulator

Our strategy selected to analyze the EC of LIRs is a hybrid modeling approach consisting of a data- and process-driven model. Firstly, this section proposes a process-driven model based on the EC of the components of the robot.

Based on the manuals and user guides from the robot manufacturers [20], [21], [22] and on the mathematic models for manipulators presented by [17], [18], we observed five consumer groups that use energy on a manipulator. The total EC of a manipulator depicted by Fig. 1 is defined as

$$E_R = E_E + E_B + \Delta E_K + \Delta E_P + L_M + L_E\,, \qquad (1)$$

where E_E, E_B, ΔE_K, ΔE_P, L_M, and L_E denote the EC of electronic components, chopper resistor, variation of kinetic energy, variation of potential energy, mechanical losses, and electrical losses. In the following, the consumer groups are explained in detail and defined.

A. Electronic Components' Consumption (E_E)

This consumer group corresponds to the EC of any component of the robot that consumes electrical energy except motors, brakes, and braking resistor, such as components of the electrical and electronic boards, microcontrollers, sensors, electronic drivers, pendants, and onboard computers.

The Onboard Computer is responsible for communicating with all joints, ensuring safety procedures, managing on-robot programming, and interfacing with external computers. The Power Supply Unit converts the input energy source, typically AC, to the DC form used by all electronic components. The pendant, a touchscreen device, facilitates communication with the onboard computer. The robot's sensors monitor various operational parameters in the controller (temperature, voltage, current), each joint (torque, current, encoder, motor temperature), and the end effector (force and torque). Modern robots feature microcontrollers within each joint that interpret motor sensor data, execute low-level motor control, and emit high-frequency control electrical signals. Additionally, the robotic system houses general electronic components, such as LEDs, resistors, capacitors, voltage regulators, and inductors. To enhance functionality, some manufacturers have integrated additional devices, including cameras, extra sensors, and input-output electrical ports.

B. Output Mechanical Energy ($E_M = \Delta E_k + \Delta E_P$)

As output energy, we define the energy required to accelerate and decelerate the robot's rigid body and its payload. This component of EC is equal to the variation of the potential and kinematic energy of the system. The mechanical losses and output energy can be obtained by multiplying the joint electromagnetic torque $\tau_i(t)$, which includes the friction torque, by the joint velocity $\dot{\theta}_i(t)$, i.e.,

$$\begin{aligned} E_M + L_M &= \Delta E_K + \Delta E_P + L_M \\ &= \sum^{N} \int \tau_i(t) \cdot \dot{\theta}_i(t) dt\,, \end{aligned} \qquad (2)$$

such that

$$E_R = E_E + E_B + L_E + \sum^{N} \int \tau(t_i) \dot{\theta}_i(t) dt\,. \qquad (3)$$

Additionally, the positive mechanical output energy, denoted as E_M^+, is defined as the comprehensive energy needed to accelerate

(an increase in kinetic energy) and elevate (an increase in potential energy) the mechanical structure and payload. This definition takes into account mechanical losses. In essence, this value quantifies the energy that the source must supply to successfully complete the task, such that

$$P_i = \begin{cases} \tau_i(t) \cdot \dot{\theta}_i(t) & \text{if} \tau_i(t) \cdot \dot{\theta}_i(t) > 0 \\ 0 & \text{if} \tau_i(t) \cdot \dot{\theta}_i(t) < 0 \end{cases}, \tag{4}$$

$$E_M^+ = \sum^N \int P_i(t) dt \,. \tag{5}$$

C. Mechanical Losses (L_M) [23], [24]

This energy is the work required by the motors to overcome friction and windage forces and depends on the joint velocities.

Viscous Friction: The viscous friction caused by the shear stress of fluid layers depends on motor relative velocity, i.e, this friction is zero when the motor is stopped and it rises as soon as the velocity increases. Thus, this motor power loss P_V depends on the robot velocity $\dot{\theta}$ and is proportional to the square of the joint velocity by a factor f_v, such that $P_V = f_v \, \dot{\theta}^2$.

Coulomb Friction: Unlike viscous friction, Coulomb friction occurs between two contacting rigid surfaces. The magnitude of this friction depends on the normal force applied to the contact location and surface properties of the contacting materials, and its direction is inverse of motor motion direction. Thus, this power loss P_S is proportional by a factor f_c to the absolute value of the velocity, such that $P_S = f_c \, |\dot{\theta}| + f_o \, \dot{\theta}$.

Windage: Windage denotes the power loss due to the air resistance around the motor. The power consumption is proportional to the cube of the velocity by a factor f_W, such that $P_W = f_W \, \dot{\theta}^3$.

Overall, the mechanical losses depend on the motor velocities and thus on the robot's trajectory. Trajectories that generate slow motion or minimize the required motor deflection consume less energy.

Finally, the overall mechanical loss becomes

$$L_M = \sum^N \int \tau_{fi}(t) \cdot \dot{\theta}_i(t) dt \,, \tag{6}$$

$$\tau_{fi} = fv_i \cdot \dot{\theta}_i + fc_i \cdot sign(\dot{\theta}_i) + fo_i + fw_i \, \dot{\theta}_i^2, \tag{7}$$

where fv_i, fc_i, fo_i, fw_i, and N represent viscous friction coefficient, Coulomb friction coefficient, Coulomb friction offset, windage friction coefficients, and a number of joints, respectively.

D. Electrical Losses (L_E) [23], [24]

This consumer group contains the energy losses during the electromechanical energy transformation by the motors, such as copper losses, iron losses, stray losses, and switching losses. The amount of these losses depends on the motor currents, as explained in more detail.

Copper losses: As copper losses we define the energy losses occurring due to the resistance of the winding cooper. These losses are proportional to the square of the DC input current I and the cooper resistance R, such that $P_{co} = R \cdot I^2$.

Iron Losses: Iron losses occur mostly in the stator and rotor and are related to magnetic field dissipation. These losses depend on the maximum flux density (B), which is determined by coil material and its manufacturing, and on the switching frequency (f), such that $P_{Fe} = f(B, f)$.

Stray Losses: These losses arise from the non-uniform distribution of a current in copper. The stray losses are defined by $P_{SL} = k_{SL} I^x$, where k_{SL}, I, and x are the stray constant, motor current, and a parameter to be defined by experimental evaluation.

Switching Losses: These losses are related to the motor driver and proportional by the factor k_{SW} to the absolute value of the motor current I, such that $P_{SW} = k_{SW}|I|$.

$$L_E = \sum^N \int (v_i(t) \cdot i_i(t) - \tau_i(t) \cdot \dot{q}_i(t)) dt \,, \tag{8}$$

where $v_i(t)$, $i_i(t)$, $\dot{q}_i(t)$, and $\tau_i(t)$ denote voltage, current, velocity, and torque of the joint i. However, most of the robots do not have a current and voltage sensor in the motor and this value can not be measured. Instead, we can apply (3) to determine the electrical losses such that

$$L_E = E_R - E_E - E_B - \sum^N \int \tau(t_i) \dot{\theta}_i(t) dt \,. \tag{9}$$

E. Braking Consumption E_B

The robot dissipates kinetic and potential energy using two subsystems:

Mechanical Brakes E_{MB}: These devices hold joint positions while the robot is stopped and unpowered, and provide dynamic stopping in an emergency event. When the brake coils are magnetized, the disk brake is released allowing the joint to move. The brake coils' consumption is independent of the motor current, speed, or position, and is constant while the brake disk is released.

Regenerative Brakes E_{RB}: Robots possess a chopper resistor that regulates the voltage of the DC bus. When the robot reduces its kinematic energy or potential energy, motors behave like generators that return energy to the system increasing the DC bus voltage. This resistor transforms unused energy into heat keeping the voltage in a safe range. If the DC bus increases, the electronic components might not function properly or get damaged. The energy dissipated by this resistor is estimated by the negative mechanical power, which represents the energy to decelerate the manipulator structure and payload,

$$P_i^- = \begin{cases} -\tau_i(t) \cdot \dot{\theta}_i(t) & \text{if} \tau_i(t) \cdot \dot{\theta}_i(t) < 0 \\ 0 & \text{if} \tau_i(t) \cdot \dot{\theta}_i(t) > 0 \end{cases}, \tag{10}$$

$$E_{RB} = \sum^N \int P_i^-(t) dt \,. \tag{11}$$

The regenerated energy is used by the motor to compensate for the electrical losses or the consumption of other components, i.e., this energy can be dissipated before it reaches the resistor [25]. An additional power sensor is required to differentiate between the regenerative braking energy and the electrical losses. To avoid the use of additional hardware, we cluster the electrical losses and regenerative braking energy in only one term, such that

$$L_E^* = L_E + E_{RB} \,, \tag{12}$$

and this term is estimated using the following equation

$$L_E^* = E_R - E_E - E_{MB} - \sum^N \int \tau(t_i) \dot{\theta}_i(t) dt \,. \tag{13}$$

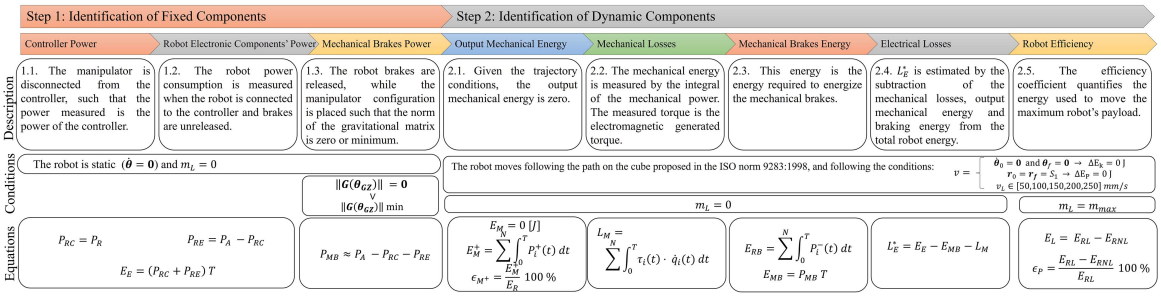

Fig. 2. ECDP: this method is based on two steps to identify five consumer groups. The figure summarizes method procedures and equations to quantify the energy of each consumer group.

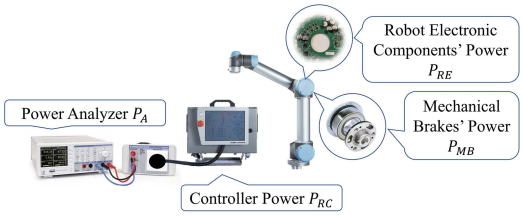

Fig. 3. Power measurements for fixed energy consumption: electronics' components consumption E_E and mechanical brakes consumption E_{MB}.

IV. The Energy Consumption Disaggregation Pipeline

Based on the theoretical disaggregation of the system EC we suggest a pipeline to experimentally identify the major subsystems' energy consumption. The approach is depicted in Fig. 2 and the required steps are explained in detail in the following.

A. Step 1: Identification of Fixed Energy Components

The robot is composed of two fixed consumer groups, i.e, electronics components' consumption E_E and mechanical brakes E_{MB}, as it is shown in Fig. 3.

The energy consumption E_E can not be precisely measured by non-intrusive methods. To disaggregate the EC of each E_E subcomponent, additional sensors are required in each of these elements. In this letter, we propose a method to estimate the E_E while the robot is stationary. Even when the robot is stationary it still computes operations to maintain the manipulator position. Besides, the robot was tested using low-expensive computing activities using basic high-level robot commands. Therefore, we assume that the consumer group E_E is similar in standby position and during the robot operation.

1) Electronics Components' Consumption E_E: The electronics components such as sensors, cameras, and other peripherals are located in the controller and manipulator. We differentiate the energy consumption of these subconsumer groups:

Controller Power (P_{RC}): The energy of the controller box is measured when the manipulator is disconnected from the controller. Therefore, the power consumption of the controller P_{RC} is equal to the electrical power measured by the power analyzer P_A. This measurement corresponds to the consumption of the onboard computer, energy source, internal sensors, electronic elements of controller electrical boards, pendant, and any additional device connected to the controller.

Robot Electronic Components' Power (P_{RE}): The manipulator is connected to the controller, but the robot is static and the brakes are not released. Motors are inactive and do not consume any energy. The power consumption P_A is measured, and the power P_{RE} is calculated by $P_{RE} = P_A - P_{RC}$.

The EC of this consumer group E_E depends on the Controller Power P_{RC}, Robot Electronic Components' Power P_{RE}, and operation time T, such that:

$$E_E = (P_{RC} + P_{RE})\,T\,. \tag{14}$$

2) Mechanical Brakes' Power (P_{MB}): In this step, the brakes are released, and the robot remains static in a given configuration denoted as θ_{GZ}. Since the robot is static, the output mechanical energy and mechanical losses are both zero. However, to compensate for gravitational forces, the motors are activated while the brakes are released and generate torque. To minimize motor EC, the robot should be positioned in a way that eliminates or minimizes the manipulator gravitational matrix norm ($\|G(\theta_{GZ})\|$), which is determined using the dynamic model of the manipulator, i.e.,

$$\theta = \{\theta_{GZ} \in \mathbb{R}^n \,/\, \|G(\theta_{GZ})\| = 0 \vee \|G(\theta_{GZ})\|_{\min}\}\,, \tag{15}$$

where θ_{GZ} is the joint configuration that minimizes or eliminates the gravitational torque matrix norm for a n DoF manipulator.

Given the experimental conditions, the robot only consumes energy due to its brakes (P_{MB}) and electronic components ($P_{RC} + P_{RE}$). As a result, the mechanical brakes' power P_{MB} is estimated by

$$P_{MB} \approx P_R - P_{RC} - P_{RE}\,. \tag{16}$$

B. Step 2: Identification of Variable Energy Components

For the identification of the remaining consumer groups, the robot needs to move. The design of the trajectory will likely influence the measurements such that we define a standardized measurement trajectory considering that:

1) The initial and final configurations are the same. Therefore, there is no variation of potential energy ($\Delta E_p = 0$).
2) The initial and final velocity is zero. Thus, there is no variation of kinematic energy ($\Delta E_k = 0$).

To accurately determine the mechanical output energy of a robot, kinematic and potential energy models must be developed based on the joint configuration of the robot structure and payload. However, the accuracy of the energy disaggregation process relies heavily on the accuracy of the model. To circumvent the need for additional models, a trajectory can be defined where the initial and final joint configurations are similar and the initial and final joint velocities are null. Please note that our study's focus is on the scenario where E_M is zero, as it simplifies the experimental procedure while still providing valuable insights. However, we acknowledge that future research could explore cases with non-zero mechanical output energy, which would require more sophisticated modeling.

The reference cube provided by ISO 9283:1998 is used to define the robot's path [26]. Therefore the proposed measurement trajectory becomes $S_1 \rightarrow P_1 \rightarrow P_2 \rightarrow P_3 \rightarrow P_4 \rightarrow S_1$. Fig. 4

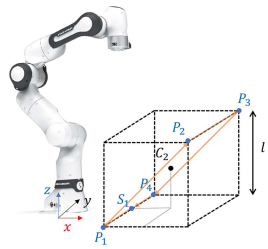

Fig. 4. Robot path for the Pipeline Step 2. The robot follows the path $\overline{S_1P_1P_2P_3P_4}$. The size length l and the center point C_2 are defined according to the ISO norm 9283:1998 [26].

shows the robot's path. We evaluate the EC using five average linear Cartesian velocities $v_L \in [50, 100, 150, 200, 250]$ mm/s to observe the influence of the speed in the mechanical and electrical losses. The experiment is a non-intrusive method that relies on the internal sensors of each robot and a power analyzer. The joint velocities, torque, and robot's EC should be saved in a data set. Following the criteria proposed by ISO 9283:1998 for test methods, we recommend that this experiment should be repeated 30 times.

Using the information collected from the dynamic experiment, we determine the consumer groups E_M^+, L_M, E_{MB}, and L_E^*.

Mechanical Output Energy E_M: The mechanical output energy E_M of the system is zero $E_M = 0[J]$, because of the experiment conditions $\Delta E_K = 0$ and $\Delta E_P = 0$, i.e, all the energy given to the motors to accelerate is returned when motors decelerate. However, the positive mechanical energy E_M^+ can be estimated using (5). Then, motion efficiency coefficient ϵ_{M^+} is calculated using:

$$\epsilon_{M^+} = \frac{E_M^+}{E_R} 100\% \,. \tag{17}$$

This index represents the relation between the mechanical energy required to accelerate the robot structure E_M^+ and the total energy used by the robot E_R.

Mechanical Losses L_M: To estimate the mechanical losses L_M, (2) is modified considering the experimental conditions $\Delta E_p = 0$ and $\Delta E_k = 0$. This results in:

$$L_M = \sum^{N} \int \tau_i(t) \cdot \dot{\theta}_i(t) dt \,. \tag{18}$$

Mechanical Brakes' Energy E_{MB}: using the mechanical brakes power P_{MB} from the step 1, the mechanical brakes' energy E_{MB} is estimated by

$$E_{MB} = T\, P_{MB} \,. \tag{19}$$

The regenerative braking energy E_{RB} is estimated using (11). However, this energy can be dissipated in other components before it reaches the braking resistor.

Electrical Losses L_E^*: Known the braking energy, electronic components energy, and mechanical data from the trajectory (joint torques and velocities), the electrical losses are determined using (13).

Payload Efficiency Coefficient ϵ_P: Experimentally, the energy required to move a payload for a given robot can be estimated by

$$E_P = E_{RL} - E_{RNL} \,, \tag{20}$$

where E_{RL}, and E_{RNL} are the manipulator's EC with and without payload, respectively. Then, the efficiency coefficient ϵ_P is obtained by the relation of the output energy E_P by the input energy E_{RL}, such that

$$\epsilon_P = \frac{E_{RL} - E_{RNL}}{} \,. \tag{21}$$

The coefficient ϵ_P reflects the system's efficiency to move a payload in the given trajectory. The payload weight influences this metric, as a higher payload would result in a higher ϵ_P. To examine the robot's performance under extreme conditions, we conducted tests with the robots lifting their maximum payload weight. This approach allows for a fair and meaningful comparison across different designs while pushing the systems to their limits.

V. Case Study

A. Materials

The following devices and components are required to implement the disaggregation pipeline:

Power Analyzer: This device measures the EC of the whole robot (P_R^*). The power analyzer HMC8015 from Rohde Schwarz was selected. This device's maximum voltage input is 600 VRMS and the maximum current input is 20 A. According to the manufacturer's datasheet, the robot UR10e, which consumes the most energy, uses maximum 615 W. Therefore, the power analyzer can measure the power consumption of the four robots.

Weights: a set of normed weights is used as the payload. For the experiments, payloads of 3 kg, 4 kg, 5 kg, and 10 kg were utilized for the robots FR3, Gen3, UR5e, and UR10e, respectively.

Robot and Controller Box: The pipeline is tested using four robots UR10e, UR5e, Franka Emika FR3, and Kinova Gen3, as it is shown in Fig. 5. The Franka FR3 is a seven-degrees-of-freedom manipulator with 3 kg of payload. The Universal Robot UR3e and UR10e are six-degree-of-freedom manipulators with 5 kg and 10 kg of payload. Finally, the Kinova Gen3 is a seven-degrees-of-freedom manipulator with 4 kg of payload.

Torque sensing: The pipeline highly depends on the velocity and torque measurements. It is required that the torque measurements represent the electromagnetic joint torque, which includes the friction torque. The robots FR3 and Gen3e have an integrated torque sensor that measures this magnitude. However, there are some losses due to the coupling between the sensor and the motor axis that can not be measured. For UR robots, joint torque estimation relies on motor currents and the motor model, but indirect measurement procedures can introduce discrepancies in the results due to potential model issues.

The procedure uses the robots' integrated Cartesian controllers and the interfaces that are available to any user. To command the controllers and measure joint torque and velocity, we use the manufacturer interfaces, i.e., Real-Time Data Exchange (RTDE), Franka Control Interface (FCI), and Kinova Kortex. All tests are started with the robots' run time on this day being $\approx$ 10 min, to ensure comparable motor temperature among the robots.

Please note, that this letter does not provide a representative energy performance evaluation for an entire robot series, but evaluates the performance of the considered individual robots mentioned above.

B. Robot Paths

The robot path is defined based on the reference cube following ISO 9283:1998 [26]. According to the norm, each robot has its own cube dimensions, determined by its working area, and is defined by a central point C_2 and a side size l_c. The side size is 400 mm for the Franka FR3, Kinova Gen3, and UR5e, and 800 mm for the UR10e. All points are defined and listed in Table I.

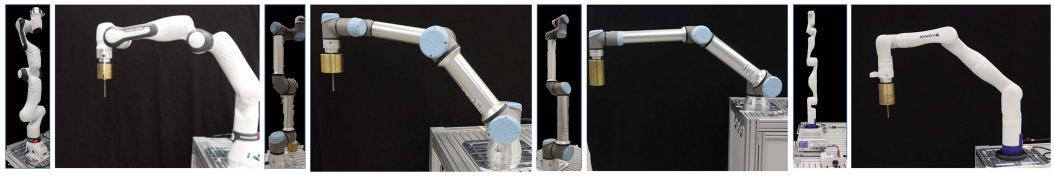

Fig. 5. ECDP was tested using four manipulators, e.g., Franka FR3, Universal Robot UR5e, UR10e, and Kinova Gen 3e, left to right. The payload weights of these robots are $m_{FR3} = 3\,\text{kg}$, $m_{UR5e} = 5\,\text{kg}$, $m_{UR10e} = 10\,\text{kg}$, and $m_{Gen3} = 4\,\text{kg}$.

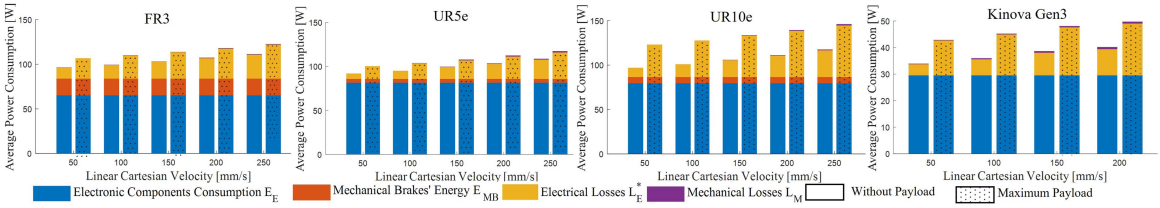

Fig. 6. Average Power Components of each robot of the consumer groups for the four robots.

TABLE I
CUBE POINTS BASED ON ISO 9283:1998

Robot	Franka FR3	U5e	UR10e	Kinova Gen3e
lc [mm]	400	400	800	400
C_2 [mm]	[498,0,252]	[510,0,256]	[726,0,0]	[250,-50,0]
P_1 [mm]	[298,200,052]	[310,200,056]	[326,400,-400]	[250,-150,-200]
P_2 [mm]	[698,200,452]	[710,200,456]	[1126,400,400]	[650,350,-200]
P_3 [mm]	[698,-200,452]	[710,-200,456]	[326,-400,400]	[650,350,200]
P_4 [mm]	[298,-200,052]	[310,-200,056]	[1126,-400,-400]	[250,-150,200]

TABLE II
ELECTRONIC COMPONENTS' CONSUMPTION

Robot	P_{RC} [W]	P_{RE} [W]	P_E [W]	P_{MB} [W]
FR3	32.12	33.09	65.21	18.6436
UR5e	54.03	27.38	81.41	4.3669
UR10e	52.29	26.27	78.56	6.9176
Kinova Gen3e	-	-	29.54	0

C. Results

Pipeline Step 1 identifies the electronic components power P_E and mechanical brake power P_{MB}. In Table II, the power of the controller, manipulator electronic components, and brakes is presented.

FR3 electronic components consume the most energy. Also, this manipulator is the one that consumes the most power for mechanical brakes P_{MB}. Nevertheless, these results are influenced by the fact that this robot has seven joints, one more joint than UR robots. UR controllers consume the most power P_{RC} of the four robots, which also includes the teach pendant attached to the controller box. In the case of the robot Kinova Gen3, the controller is fixed to the robot. The method can not measure separately the power of the controller P_{RC} and the robot electronics P_{RE}. Kinova Gen 3 consumes the least electronic components power P_E (29.54 W). It should be noted that this manipulator does not have brakes and, thus, $P_{MB} = 0$.

Pipeline Step 2 identifies the four robots' mechanical losses, electrical losses, braking energy, and electronic consumption. The results are presented in Table III for the robots Franka FR3, UR5e, UR10e, and Kinova Gen. Fig. 6 presents the average power of each consumer group, and Fig. 8 summarizes the information using comparative absolute and relative charts. To compare the consumption of the consumer groups, we compare the percent of EC by each consumer group.

On average 67.76% of the total energy of all robots is used for energizing the electronic components P_E (57-82%). This consumer group power is fixed, i.e., it does not directly depend on the robot's motion, trajectory, or payload. This consumer group depends on the operation time T.

The electrical losses L_E^* is the next consumer group, which constitutes 13-39% of the total robot energy, on average 23.84%. The significance of L_E^* rises when the Cartesian velocity and the payload increase. In our comparison, the UR10e consumes the largest percent of electrical losses power (28.22% - 33.21 W), and Kinova Gen3 the least (27.62% - 11.79 W). The EC due to robot motor brakes P_{MB} is the third consumer group, which has different tendencies in each robot. The braking power P_{MB} of FR3 is the highest of the four robots (17.12% - 18.64 W). Kinova Gen3 consumes the least power (0%), since Kinova Gen3 does not have mechanical brakes ($P_{MB} = 0$).

The mechanical losses in all cases are less than 1% of the total energy. The method depends on the torque measurements to define the mechanical losses. As the UR robots perform torque estimation based on the motor current imprecision occurs in the torque estimation. These imprecise torque values result in negative values of mechanical losses for UR5e and UR10e in Table III. The coefficient ϵ_{M+} is less than 8% in every case. This coefficient reflects how much of the total input energy is transformed into mechanical energy. However, the accuracy of this value for robots UR5e and UR10e is doubtful because this coefficient is also affected by the joint torque measurements. The motion efficiency coefficient ϵ_{M+} increases when the robot moves faster. The robots are divided into two groups according to the coefficient ϵ_P. The robots UR5e and FR3 have a coefficient of 9.51% and 7.92%, respectively. In the second group, there are the robots UR10 and Kinova Gen3 20.50% and 20.16%, respectively. Fig. 7 shows the electrical power of each consumer group on time. These graphs present the average power of the 30 repetitions in each experiment. In all the samples, the valleys of the graphs are located close to the cube corners. The robot power P_R increases when the robot accelerates and decreases when the robot decelerates. The mechanical power is negative when the robot goes from point P_3 to P_4 because potential energy is restored to the system. In this motion, there is a negative variation in height, i.e. downward motion, and therefore, the robot returns energy to the system. Fig. 8 summarizes the results for each robot with and without payload and gives the general results for all the robots. On average, consumer groups' electronics consumption, braking energy, electrical losses, and mechanical losses consume 68.78%, 6.77%, 23.84%, and 0.60% of the total power, respectively.

TABLE III
ENERGY COMPONENTS WITH AND WITHOUT PAYLOAD FOR ROBOTS FR3, UR5E, UR10E, AND GEN3

	v_R	Without Payload m = 0 [kg]										Maximum Payload [a]										$E_{RNL} - E_{RL}$	
	mm/s	E_{RNL} [J]	E_E [J]	%	E_B [J]	%	L_E^* [J]	%	L_M [J]	%	ϵ_{M+} %	E_{RL} [J]	E_E [J]	%	E_B [J]	%	L_E^* [J]	%	L_M [J]	%	ϵ_{M+} %	[J]	ϵ [%]
FR3	50	3719.7	2518.9	67.7	720.0	19.4	476.4	12.8	4.3	0.1	1.7	4128.3	2518.9	61.0	720.0	17.4	884.8	21.4	4.5	0.1	2.6	408.6	9.9
	100	1917.7	1259.5	65.7	360.0	18.8	293.9	15.3	4.3	0.2	3.4	2126.0	1259.5	59.2	360.0	16.9	501.9	23.6	4.6	0.2	5.0	208.3	9.8
	150	1326.9	839.6	63.3	240.0	18.1	243.0	18.3	4.2	0.3	4.9	1465.5	839.6	57.3	240.0	16.4	381.1	26.0	4.7	0.3	7.3	138.6	9.5
	200	1035.2	629.7	60.8	180.0	17.4	221.1	21.4	4.4	0.4	6.3	1139.3	629.7	55.3	180.0	15.8	324.9	28.5	4.7	0.4	9.5	104.1	9.1
	250	859.5	503.8	58.6	144.0	16.8	207.4	24.1	4.3	0.5	7.7	947.3	503.8	53.2	144.0	15.2	294.9	31.1	4.6	0.5	11.5	87.8	9.3
				63.2		18.1		18.4		0.3	4.8			57.2		16.4		26.1		0.3	7.2		9.5
UR5e[b]	50	3542.8	3145.6	88.7	168.8	4.8	234.9	6.6	-4.7	-0.1	0.1	3870.1	3145.6	81.2	168.8	4.4	555.1	14.3	2.3	0.1	1.7	327.3	8.5
	100	1836.0	1572.8	85.7	84.4	4.6	178.8	9.7	-0.1	-0.0	0.4	2002.3	1572.9	78.6	84.4	4.2	338.2	16.9	6.6	0.3	3.7	166.4	8.3
	150	1281.9	1048.6	81.8	56.3	4.4	173.9	13.6	3.1	0.2	0.8	1385.0	1048.6	75.7	56.3	4.1	270.5	19.5	9.7	0.7	5.7	103.1	7.4
	200	998.0	786.6	78.9	42.2	4.2	164.4	16.5	4.2	0.4	1.1	1084.1	786.5	72.6	42.2	3.9	243.5	22.5	11.9	1.1	7.6	86.0	7.9
	250	838.5	629.3	75.1	33.8	4.0	168.6	20.1	6.7	0.8	1.6	906.2	629.3	69.4	33.8	3.7	230.2	25.4	13.9	1.5	9.4	67.7	7.5
				82.0		4.4		13.3		0.3	0.8			75.5		4.1		19.7		0.7	5.6		7.9
UR10e[b]	50	7485.4	6147.4	82.1	534.6	7.1	808.2	10.8	-4.6	-0.1	0.3	9494.4	6147.3	64.7	534.6	5.6	2814.9	29.6	-2.4	-0.0	0.3	2009.1	21.2
	100	3904.6	3073.8	78.7	267.3	6.8	559.5	14.3	4.1	0.1	0.8	4932.3	3073.8	62.3	267.3	5.4	1585.7	32.1	5.5	0.1	0.6	1027.8	20.8
	150	2727.7	2049.2	75.1	178.2	6.5	493.1	18.1	6.7	0.2	1.3	3438.8	2049.3	59.6	178.2	5.2	1194.9	34.7	16.4	0.5	1.0	710.3	20.7
	200	2145.4	1537.0	71.6	133.7	6.2	465.1	21.7	9.4	0.4	1.9	2693.4	1537.0	57.1	133.7	5.0	1002.8	37.2	19.9	0.7	1.4	548.0	20.3
	250	1817.1	1229.6	67.7	106.9	5.9	463.4	25.5	17.4	1.0	2.8	2255.6	1229.6	54.5	106.9	4.7	897.9	39.8	21.2	0.9	1.9	440.1	19.5
				75.1		6.5		18.1		0.3	1.4			59.6		5.2		34.7		0.5	1.1		20.5
Gen3	50	1300.1	1133.6	87.2	0.0	0.0	159.6	12.3	6.9	0.5	1.7	1642.7	1133.7	69.0	0.0	0.0	503.0	30.6	6.1	0.4	3.2	342.6	20.9
	100	691.6	568.7	82.2	0.0	0.0	115.3	16.7	7.6	1.1	3.2	871.2	568.6	65.3	0.0	0.0	296.0	34.0	6.5	0.7	6.2	179.5	20.6
	150	494.3	378.2	76.5	0.0	0.0	108.0	21.9	8.1	1.6	4.4	616.8	378.7	61.4	0.0	0.0	231.4	37.5	6.7	1.1	8.8	122.5	19.9
	200	392.0	288.1	73.5	0.0	0.0	95.5	24.4	8.3	2.1	5.1	485.8	288.6	59.4	0.0	0.0	190.1	39.1	7.1	1.5	10.5	93.8	19.3
				79.9		0.0		18.8		1.4	3.6			63.8		0.0		35.3		0.9	7.2		20.2

[a] Maximum payload : $m_{Fr3e} = 3\,\text{kg}$, $m_{UR5e} = 5\,\text{kg}$, $m_{UR10e} = 10\,\text{kg}$, $m_{UR10e} = 4\,\text{kg}$.
[b] This robot does not have torque sensors, the torque measurements are estimated using the motor current.

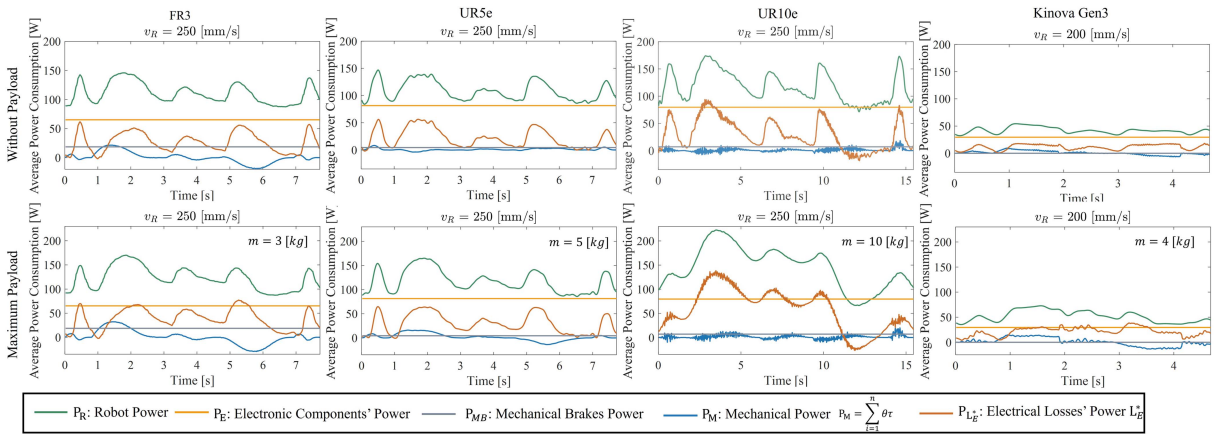

Fig. 7. Power components on time P_R, P_E, P_M, $P_{L_E^*}$, and P_{MB} represent the power of the robot, electronic components, mechanical energy (including the mechanical losses and mechanical output energy), electrical losses, and the mechanical brakes' power, respectively.

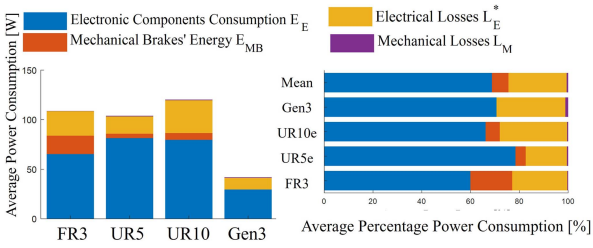

Fig. 8. Average power consumption per robot of all the repetitions with and without payload. The left figure shows the absolute power and the right figure shows the relative percent power per consumer group.

VI. DISCUSSION

Optimization techniques for traditional IRs have primarily focused on reducing mechanical energy, mechanical losses, and electrical losses through trajectory and path planning. However, for LIRs, electronic components are the principal energy spender, as shown in Fig. 8. Therefore, traditional optimization methods used for IRs would not have the same impact on LIRs. To reduce energy consumption in LIRs, optimization methods need to focus on exploring solutions that address the electronic design and components used by different manufacturers. A more-detailed analysis is necessary, as there are many components included in this consumer group. One approach is to determine the energy ratio of each electronic component and focus on reducing the energy consumption of the most significant components. Another solution is to establish an efficient electronic design software architecture that considers the required computing capacity of the controllers and to decentralize expensive computing tasks to cloud services. By doing so, the powerful robot controller can be replaced by microcontrollers, leading to potential energy savings. Thus, a more targeted approach is needed when exploring optimization methods for LIRs to ensure energy efficiency while accounting for the diverse electronic designs and components used by different manufacturers.

It is important to note that the EC of the electronics is defined by the hardware and software design of the system. This means

that a common user of off-the-shelf robots cannot change this design. However, the results of our study can still serve as a motivation for manufacturers to invest in improving their hardware and software design, which can ultimately lead to more energy-efficient robots in the future.

One limitation of our study is that the method cannot distinguish between electrical losses and regenerative braking energy as this would require an additional power sensor incorporated into the robot. Also, the accuracy of our calculation of mechanical losses depends on the robot-embedded torque sensing. For this study, we assume that for all considered robot systems the measured torque is the joint-generated torque, including the friction torque. However, using the same standardized torque sensor in every robot system's joints certainly improves the accuracy of our calculation. Lastly, we assume that the energy consumption of the electronics remains constant over time. An additional sensor is required to measure the effects of time on its power consumption. While for the presented ECDP the focus is on a general comparison of energy consumers in the LIR and providing an easily reproducible measurement setup, more extensive experiments can be conducted to enhance the precision of our calculation pipeline.

VII. Conclusion

In this letter, we present the Energy Consumption Disaggregation Pipeline (ECDP) for disaggregating the energy consumption of any mechatronic system. To demonstrate the ECDP, we focus on lightweight industrial robots (LIRs) and provide reproducible measurement setups and protocols for quantifying their energy components. Our method has limitations, such as differentiating between electrical losses and regenerative braking energy, relying on the robot's torque measurements, and measuring the constant energy consumption of electronics, which can be addressed with additional internal invasive sensors. The method was tested using four LIRs, namely, FR3, UR5e, UR10e, and Kinova Gen3. On average, the results showed that consumer groups' electronics consumption, braking energy, electrical losses, and mechanical losses consume 68.78%, 6.77%, 23.84%, and 0.60% of the total power, respectively. This shows that electronic components consume the most energy in the robot, while mechanical losses due to robot motion design constitute lowly to LIRs energy consumption. Therefore, the approaches required to optimize the energy consumption of LIRs differ significantly from traditional approaches for industrial robots. Instead of focusing on reducing mechanical energy, mechanical losses, and electrical losses through path and trajectory planning, energy consumption optimization for LIRs should concentrate on the electronic design and its components. One strategy could be to efficiently distribute computation tasks across the system assets.

References

[1] IFR, "World robotics 2022 report," International Federation of Robotics, Frankfurt, Germany, Tech. Rep. 2022, 2022.

[2] R. Bogue, "Europe continues to lead the way in the collaborative robot business," *Ind. Robot: An Int. J.*, vol. 43, pp. 6–11, 2016.

[3] M. Gadaleta, G. Berselli, M. Pellicciari, and F. Grassia, "Extensive experimental investigation for the optimization of the energy consumption of a high payload industrial robot with open research dataset," *Robot. Comput.-Integr. Manuf.*, vol. 68, Jul. 2021, Art. no. 102046.

[4] M. Brossog, J. Kohl, J. Merhof, S. Spreng, and J. Franke, "Energy consumption and dynamic behavior analysis of a six-axis industrial robot in an assembly system," *Procedia CIRP*, vol. 23, pp. 131–136, 2014.

[5] A. Liu, H. Liu, B. Yao, W. Xu, and M. Yang, "Energy consumption modeling of industrial robot based on simulated power data and parameter identification," *Adv. Mech. Eng.*, vol. 10, no. 5, pp. 1–11, 2018.

[6] M. Gadaleta, M. Pellicciari, and G. Berselli, "Optimization of the energy consumption of industrial robots for automatic code generation," *Robot. Comput.- Integr. Manuf.*, vol. 57, pp. 452–464, 2019.

[7] A. Mohammed, B. Schmidt, L. Wang, and L. Gao, "Minimizing energy consumption for robot arm movement," *Procedia CIRP*, vol. 25, pp. 400–405, 2014.

[8] D. Meike, M. Pellicciari, G. Berselli, A. Vergnano, and L. Ribickis, "Increasing the energy efficiency of multi-robot production lines in the automotive industry," in *Proc. IEEE Int. Conf. Automat. Sci. Eng.*, 2012, pp. 700–705.

[9] A. Vergnano et al., "Modeling and optimization of energy consumption in cooperative multi-robot systems," *IEEE Trans. Automat. Sci. Eng.*, vol. 9, no. 2, pp. 423–428, Apr. 2012.

[10] D. Meike, M. Pellicciari, and G. Berselli, "Energy efficient use of multi-robot production lines in the automotive industry: Detailed system modeling and optimization," *IEEE Trans. Automat. Sci. Eng.*, vol. 11, no. 3, pp. 798–809, Jul. 2014.

[11] M. Pellicciari, G. Berselli, F. Leali, and A. Vergnano, "A method for reducing the energy consumption of pick-and-place industrial robots," *Mechatronics*, vol. 23, no. 3, pp. 326–334, 2013.

[12] A. H. Sabry, F. H. Nordin, A. H. Sabry, and M. Z. A. A. Kadir, "fault detection and diagnosis of industrial robot based on power consumption modeling," *IEEE Trans. Ind. Electron.*, vol. 67, no. 9, pp. 7929–7940, Sep. 2020.

[13] A. Rassõlkin, H. Hõimoja, and R. Teemets, "Energy saving possibilities in the industrial robot IRB 1600 control," in *Proc. IEEE 7th Int. Conf.-Workshop Compat. Power Electron.*, 2011, pp. 226–229.

[14] R. R. Garcia, A. C. Bittencourt, and E. Villani, "Relevant factors for the energy consumption of industrial robots," *J. Braz. Soc. Mech. Sci. Eng.*, vol. 40, no. 9, pp. 1–15, 2018.

[15] F. Stuhlenmiller, J. Jungblut, D. Clever, and S. Rinderknecht, "Combined analysis of energy consumption and expected service life of a robotic system," in *Proc. IEEE 6th Int. Conf. Mechatron. Robot. Eng.*, 2020, pp. 53–57.

[16] S. Riazi, K. Bengtsson, O. Wigström, E. Vidarsson, and B. Lennartson, "Energy optimization of multi-robot systems," in *Proc. IEEE Int. Conf. Automat. Sci. Eng.*, 2015, pp. 1345–1350.

[17] M. Pellicciari et al., "AREUS - innovative hardware and software for sustainable industrial robotics," in *Proc. IEEE Int. Conf. Automat. Sci. Eng.*, 2015, pp. 1325–1332.

[18] J. Heredia, C. Schlette, and M. B. Kjærgaard, "Data-driven energy estimation of individual instructions in user-defined robot programs for collaborative robots," *IEEE Robot. Automat. Lett.*, vol. 6, no. 4, pp. 6836–6843, Oct. 2021.

[19] N. Batra et al., "Towards reproducible state-of-the-art energy disaggregation," in *Proc. 6th ACM Int. Conf. Syst. Energy-Efficient Buildings, Cities, Transp.*, 2019, pp. 193–202.

[20] U. Robots, "Universal robots e-series user manual," 2022. [Online]. Available: https://www.universal-robots.com/download

[21] Kinova, "User guide kinova Gen3 ultra lightweight robot," 2022. [Online]. Available: https://www.kinovarobotics.com/uploads/

[22] Franka, "Product manual franka production 3," 2022. [Online]. Available: https://www.franka.de/documents/

[23] P. Andrada, M. Torrent, J. I. Perat, and B. Blanqué, "Power losses in outside-spin brushless DC motors," *Renewable Energy Power Qual. J.*, vol. 1, no. 2, pp. 507–511, 2004.

[24] E. S. Sergaki, G. S. Stavrakakis, and A. D. Pouliezos, "Optimal robot speed trajectory by minimization of the actuator motor electromechanical losses," *J. Intell. Robot. Syst.*, vol. 33, no. 2, pp. 187–207, Feb. 2002, doi: 10.1023/A:1014643401778.

[25] T. Verstraten, R. Furnémont, G. Mathijssen, B. Vanderborght, and D. Lefeber, "Energy consumption of geared DC motors in dynamic applications: Comparing modeling approaches," *IEEE Robot. Automat. Lett.*, vol. 1, no. 1, pp. 524–530, Jan. 2016.

[26] *Manipulating Industrial Robots- Performance Criteria and Related Test Methods*, EN ISO Standard 9283:1999-05, ISO, Geneva, Switzerland, 1999.